

Normalized Modeling of Piezoelectric Energy Harvester Based on Equivalence Transformation and Unit-Less Parameters

Lucas S. Mendonça¹, Leandro T. Martins², Matthias Radecker,
Fábio E. Bisogno, and Dirk Killat, *Member, IEEE*

Abstract—Micro-electromechanical systems are ubiquitous in several energy harvesting solutions and can be used in applications such as bio-implantable devices and wireless micro-sensors. Piezoelectricity is an interesting key to perform the interface between environmental extracted energy and the power delivered to the load due to the use of mechanical vibration and resonance features. However, it is necessary for a detailed analysis in order to obtain an accurate understanding of the system. In this regard, some works deal with the normalization procedures to analyze the piezoelectric component behavior based on the mechanical resonance frequency. In order to enhance the system modeling, the electromechanical resonance frequency must also be analyzed. This paper deals with an approach to model the piezoelectric component that allows analyzing several unitless parameters that are critical to improve the performance of the system. In addition, a state-space model for the piezo-harvester based on the Class-E resonant rectifier is presented. Some experimental results are shown to validate the theoretical approach. [2019-0082]

Index Terms—Piezoelectricity, state-space models, system modeling.

I. INTRODUCTION

THE addition of mechanical elements in pure electronics evoke the born of micro electromechanical systems (MEMS), which led to improvements on integrated circuits capabilities. Several materials are used in MEMS devices, such as, silicon, glass, plastic and piezoelectric [1]. From biological structures, like bones and viruses to the well-known quartz, some piezoelectric materials are suitable for vibration-based harvesting due to their high energy density per volume and

Manuscript received April 15, 2019; revised May 17, 2019; accepted May 29, 2019. This work was supported in part by the Coordenação de Aperfeiçoamento de Pessoal de Nível Superior (CAPES/PROEX), Brazil, under Grant 001, in part by the National Council for Scientific and Technological Development (CNPq), and in part by the Division Engineering of Adaptive Systems, Fraunhofer Institute for Integrated Circuits. Subject Editor A. Holmes. (Corresponding author: Lucas S. Mendonça.)

L. S. Mendonça, L. T. Martins, and M. Radecker are with the Fraunhofer IIS/EAS, Division Engineering of Adaptive Systems, Fraunhofer Institute for Integrated Circuits, 01069 Dresden, Germany (e-mail: lucas.mendonca@eas.iis.fraunhofer.de).

F. E. Bisogno is with the Power Processing Engineering Department, Universidade Federal de Santa Maria, Santa Maria 97105-900, Brazil.

D. Killat is with Mikroelektronik, Brandenburgische Technische Universität Cottbus, 01968 Cottbus, Germany.

Color versions of one or more of the figures in this paper are available online at <http://ieeexplore.ieee.org>.

Digital Object Identifier 10.1109/JMEMS.2019.2921649

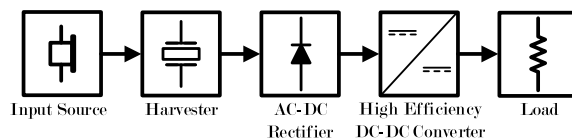


Fig. 1. Overview of an energy harvesting system.

the vast number of sources that the energy can be extracted from the environment [2], [3].

The interest of researches on piezoelectricity is founded by the growth of the number of publications [4]–[11] and innovative patents, such as, shoes equipped with piezo-harvesters [12] and bio-implantable medical devices [13], which place the piezoelectricity as an alternative energy source for low power applications. However, from the gross energy to voltage source that can supply a load, there are several building blocks that must be analyzed to improve the whole system. It can be seen in Fig. 1 that five main blocks compose the energy harvesting system. Several works aim to improve each one of them, for example, topology comparison [14], [15] and harvester modeling [16]–[18].

Regarding piezoelectric energy harvesters, several types of system representation and methodologies were explored in the literature. Exact electromechanical solution of the cantilevered piezoelectric energy harvester for transverse vibrations with Euler-Bernoulli beam assumptions can be used to analyze the system, specially to consider different scenarios, such as, harmonic base motion and harmonic base translation at an arbitrary frequency or around the natural frequency [19].

The energy conversion in vibration systems can be analyzed based on the strain distribution over the piezoelectric component length. In this case, it has been shown that segmented electrode pairs can increase the output voltage due to cancellation issue avoidance [20]. Furthermore, multi-functional piezoelectric systems were reported in the literature by means of common piezoelectric single crystals investigation in order to design a system with structural loading supporting by active devices [21].

Piezoelectric energy harvesters play a role when the goal is to improve sensors operational life time by avoiding the use of batteries. However, improvements should be taken into account, like as, the use of switch-mode interfaces circuits [22] and bi-morph modules for lane marker lighting systems [23].

Recently, microscale vibration energy harvester with high power density and ultra-low resonance frequency was reported [24]. This system provides 23.3 nW at 68 Hz excited at 0.25 g acceleration. A general methodology for analysis and design of piezoelectric metamaterials and metastructures based on root locus method was recently presented in the literature [25]. It was shown that maintaining a stable system considering many synthetic shunt circuits is a challenging task. Although, the techniques presented in [25] give a good understanding of the problem by means of several case studies.

The used analysis methodology is defined based on design factors, such as accuracy, complexity and effort. Analysis of the complete system in Fig. 1 can lead to inaccurate results in comparison with a methodology used for a single block considering the same effort. In this sense, this paper focus on the harvester and the AC-DC converter blocks in order to obtain a deep understanding of the system. Notwithstanding, the proposed method is also applied for a piezo-harvester based on Class-E resonant rectifier, which is novelty in the literature.

The main goal of this work is to develop a normalized modeling methodology based on equivalence transformation and unit-less parameters. The normalized analysis and unit-less parameters are used because they are suitable for parameter sweep and to obtain generalized solutions. Also, the equivalence transformation is used to easily convert the state-space representation based on real system parameters into an unit-less representation in a systematic way in order to obtain a state-space model that can be implemented in mathematical softwares.

Other works make use of normalizations, such as [16], [28]. However, they perform some assumptions, for example, consider only the resonance frequency between mechanical elements. Therefore, the main contribution of this work is the development of a methodology to model and analyze the piezoelectric element considering the unit-less parameters: normalized mechanical resonance frequency, normalized electromechanical resonance frequency, coupling factor, mechanical quality factor and damping factor. The unit-less parameters are extracted from the piezoelectric representation by using a decomposing in unit-less parameters scheme [29]. Also, relationships among the unit-less, electrical circuit and electromechanical parameters are derived in order to convert the generalized solutions from the modeling to real piezoelectric parameters, such as: stiffness, coupling constant, permittivity, area, mass and layer thickness. A comparison with other works and some experimental results are performed to validate the theoretical approach.

II. NORMALIZED MODELING

This section shows the normalized modeling for the piezoelectric element. First, a state-space representation based on mechanical and electrical parameters is performed (II-A). Afterwards, the equivalence transformation (II-B), the decomposition in unit-less parameters scheme (II-C) and the state-space representation based on unit-less parameters (II-D) are described step-by-step.

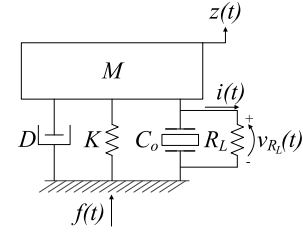


Fig. 2. Piezoelectric electromechanical representation.

A. State-Space Representation Based on Mechanical and Electrical Parameters

The piezoelectric electromechanical representation is shown in Fig. 2, in which, M is the mass, D is the mechanical damping coefficient, K is the mechanical stiffness, C_o is the piezoelectric capacitance, R_L is the load resistance, $f(t)$ is the external force, $z(t)$ is the displacement, $v_{R_L}(t)$ is the output voltage and $i(t)$ is the load current.

The governing equation of the electromechanical system is described by:

$$M \frac{d^2 z(t)}{dt^2} + D \frac{dz(t)}{dt} + K z(t) = -M \frac{d^2 y(t)}{dt^2} - \alpha v_{R_L}(t), \quad (1)$$

being, $y(t)$ the excitation displacement and α the force factor. Considering F_0 as the amplitude of the external force-voltage function, (1) can be written as:

$$\frac{d^2 z(t)}{dt^2} = -\frac{F_0 f(t)}{M} - \frac{\alpha}{M} v_{R_L}(t) - \frac{D}{M} \frac{dz(t)}{dt} - \frac{K}{M} z(t). \quad (2)$$

The governing equation of the electrical system is described by:

$$i(t) = \alpha \frac{dz(t)}{dt} - C_o \frac{dv_{R_L}(t)}{dt}. \quad (3)$$

Equation (3) can be rewritten as:

$$\frac{dv_{R_L}(t)}{dt} = \frac{\alpha}{C_o} \frac{dz(t)}{dt} - \frac{v_{R_L}(t)}{R_L C_o}. \quad (4)$$

Equations (2) and (4) are the coupled governing equations. First-order state variables must be defined as: $\mathbf{x}_1 \triangleq z(t)$, $\mathbf{x}_2 \triangleq \frac{dz(t)}{dt}$ and $\mathbf{x}_3 \triangleq v_{R_L}(t)$; in order to describe the system in a state-space form:

$$\frac{d\mathbf{x}(t)}{dt} = \mathbf{A}\mathbf{x}(t) + \mathbf{B}f(t) \quad (5)$$

and

$$\mathbf{y}(t) = \mathbf{C}\mathbf{x}(t) + \mathbf{D}f(t). \quad (6)$$

Equation (5) is the state equation, in which, \mathbf{A} and \mathbf{B} are the state and input matrices, respectively. Equation (6) is the output equation, in which \mathbf{C} and \mathbf{D} are output and transmission matrices. The state vector $\mathbf{x}(t)$ is written as:

$$\mathbf{x}(t) = [\mathbf{x}_1, \mathbf{x}_2, \mathbf{x}_3]^T. \quad (7)$$

The state and input matrices are equated as:

$$\mathbf{A} = \begin{pmatrix} 0 & 1 & 0 \\ -\frac{K}{M} & -\frac{D}{M} & -\frac{\alpha}{M} \\ 0 & \frac{\alpha}{C_o} & -\frac{1}{R_L C_o} \end{pmatrix}, \quad \mathbf{B} = \begin{pmatrix} 0 \\ -\frac{1}{M} \\ 0 \end{pmatrix}, \quad (8)$$

and the output equation matrices are going to be explained subsequently.

B. Equivalence Transformation

The model represented in (7) and (8) is dependent of real system parameters. In order to obtain a normalized model in a systematic way, an equivalence transformation, in which, the vector space described by $\mathbf{x}(t)$ is converted into a new vector space $\mathbf{e}(t)$ based on the square roots of the energy in storage elements. The new vector space is described by:

$$\mathbf{e}(t) = \left[\mathbf{x}_1 \frac{\sqrt{K}}{\sqrt{2}}, \mathbf{x}_2 \frac{\sqrt{M}}{\sqrt{2}}, \mathbf{x}_3 \frac{\sqrt{C_o}}{\sqrt{2}} \right]^T \quad (9)$$

and an equivalence transformation \mathbf{P} is obtained by:

$$\mathbf{P} = \mathbf{e}(t) \cdot \mathbf{x}(t)^{-1} = \begin{pmatrix} \frac{\sqrt{K}}{\sqrt{2}} & 0 & 0 \\ 0 & \frac{\sqrt{M}}{\sqrt{2}} & 0 \\ 0 & 0 & \frac{\sqrt{C_o}}{\sqrt{2}} \end{pmatrix}. \quad (10)$$

In order to normalize the system by the input source $\bar{\mathbf{B}}$ and considering the angular frequency ω , the new input matrix should be rewritten by:

$$\bar{\mathbf{B}} = \frac{\mathbf{P} \cdot \mathbf{B}}{\omega} = \begin{pmatrix} 0 \\ 1 \\ \frac{1}{\sqrt{2M\omega}} \\ 0 \end{pmatrix}. \quad (11)$$

The term $\frac{1}{\sqrt{2M\omega}}$ in $\bar{\mathbf{B}}$ is used to normalize the system as follows:

$$\bar{\mathbf{P}} = \frac{\sqrt{2M\omega}}{F_0} \mathbf{P}. \quad (12)$$

Matrix $\bar{\mathbf{P}}$ is the equivalence transformation that should be used to obtain a state-space model normalized by the input and angular frequency that is dependent on real circuit parameters. The following equations should be used:

$$\bar{\mathbf{A}} = \frac{\bar{\mathbf{P}} \cdot \mathbf{A} \cdot \bar{\mathbf{P}}^{-1}}{\omega}, \quad (13)$$

$$\bar{\mathbf{B}} = \frac{\bar{\mathbf{P}} \cdot \mathbf{B}}{\omega} \quad (14)$$

and

$$\bar{\mathbf{C}} = \mathbf{C} \cdot \bar{\mathbf{P}}^{-1}. \quad (15)$$

The term ω in (11), (13) and (14) is used to normalize the system in relation to the angular frequency. The new transmission matrix $\bar{\mathbf{D}}$ is the same as \mathbf{D} . At this point, it is interesting to note that \mathbf{C} is defined by the choice of interesting variables in the output vector $\mathbf{y}(\omega t)$, which in this case, $z(\omega t)$ and $v_{RL}(\omega t)$ are selected. In order to obtain the normalized output variables, $v_{RL}(\omega t)$ is parameterized by F_0 due to the equivalent circuit relation that considers force as voltage. The displacement $z(\omega t)$ should be parameterized by velocity $dz(\omega t)/dt = df_1(\omega t)/dt = \omega f_2(\omega t)$, being $f_1(\omega t)$ and $f_2(\omega t)$

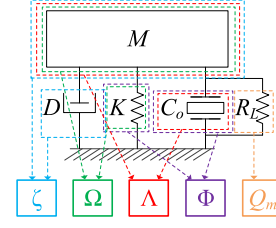


Fig. 3. Decomposition in unit-less parameters scheme.

any input functions. Considering $f_2(\omega t)$ as $z(\omega t)$, the displacement is parameterized by $\frac{\omega}{Z_0}$, being Z_0 the amplitude of the displacement function. The output vector is described as: $\mathbf{y}(\omega t) = \left[\frac{\omega z(\omega t)}{Z_0}, \frac{v_{RL}(\omega t)}{F_0} \right]^T$. Matrix \mathbf{C} is equated as following:

$$\mathbf{C} = \begin{pmatrix} \frac{\omega}{Z_0} & 0 & 0 \\ 0 & 0 & \frac{1}{F_0} \end{pmatrix}. \quad (16)$$

The new state-space matrices are obtained from (13), (14) and (15):

$$\bar{\mathbf{A}} = \begin{pmatrix} 0 & \frac{\sqrt{K}}{\sqrt{M\omega}} & 0 \\ -\frac{\sqrt{K}}{\sqrt{M\omega}} & -\frac{D}{M\omega} & -\frac{\alpha}{\sqrt{C_o M \omega}} \\ 0 & \frac{\alpha}{\sqrt{C_o M \omega}} & -\frac{1}{C_o R_L \omega} \end{pmatrix}, \quad (17)$$

$$\bar{\mathbf{B}} = \begin{pmatrix} 0 \\ 1 \\ -\frac{1}{F_0} \\ 0 \end{pmatrix} \quad (18)$$

and

$$\bar{\mathbf{C}} = \begin{pmatrix} \frac{F_0}{\sqrt{K M Z_0}} & 0 & 0 \\ 0 & 0 & \frac{1}{\sqrt{C_o M \omega}} \end{pmatrix}. \quad (19)$$

In addition, $\mathbf{D} = \bar{\mathbf{D}} = 0$ because no output variable depends on the input source. The model in (17), (18) and (19) is the state-space model normalized by the input source and the frequency that depends on real system parameters. However, this model is suitable to be converted into a normalized system that depends on unit-less parameters.

C. Decomposition in Unit-Less Parameters Scheme

Several unit-less parameters should be extracted from the system in order to represent it in a normalized manner with respect to input, frequency and system parameters. The decomposition in unit-less parameters scheme [29] is shown in Fig. 3:

The unit-less parameters are described by: damping factor, ζ ; normalized mechanical resonance frequency, Ω ; normalized electromechanical resonance frequency, Λ ; coupling factor, Φ and mechanical quality factor, Q_m .

These parameters are equated as follows:

$$\zeta = \frac{D}{2M\omega_m} = \frac{D}{2\sqrt{KM}}, \quad (20)$$

$$\Omega = \frac{\omega_m}{\omega}; \quad \omega_m = \frac{\sqrt{K}}{\sqrt{M}}, \quad (21)$$

$$\Lambda = \frac{\omega_l}{\omega}; \quad \omega_l = \frac{1}{\sqrt{C_oM}}, \quad (22)$$

$$\Phi = \frac{\alpha}{\sqrt{KC_o}} \quad (23)$$

and

$$Q_m = R_L\omega_m C_o. \quad (24)$$

Being: ω_m the mechanical resonance frequency related to K and M and ω_l the electromechanical resonance frequency related to C_o and M . Furthermore, F_0 and Z_0 can be related considering R_L and the inverse system's transfer power ratio a , which is used as an interface unit-less parameter between the input and the load: $F_0/Z_0 = aR_L$.

D. State-Space Representation Based on Unit-Less Parameters

The terms in matrices described in (17), (18) and (19) are easily re-arranged by means of (20), (21), (22), (23) and (24), as shown in the following:

- $\frac{\sqrt{K}}{\sqrt{M\omega}} = \frac{\omega_m}{\omega} = \Omega$;
- $\frac{D}{M\omega} = \frac{2M\zeta\omega_m}{\sqrt{M\omega}} = 2\zeta\Omega$;
- $\frac{\alpha}{\sqrt{C_oM\omega}} = \frac{\Phi\sqrt{KC_o}}{\sqrt{C_oM\omega}} = \frac{\Phi\sqrt{K}}{\sqrt{M\omega}} = \frac{\Phi\omega_m}{\omega} = \Phi\Omega$;
- $\frac{1}{C_oR_L\omega} = \frac{\omega_m}{\omega_m C_o R_L \omega} = \frac{\Omega}{Q_m}$;
- $\frac{F_0}{\sqrt{KM}Z_0} = \frac{aR_L}{\sqrt{KM}} = \frac{Q_m a \Omega^2}{\Lambda^2}$;
- $\frac{1}{\sqrt{C_oM\omega}} = \frac{\omega_l}{\omega} = \Lambda$.

The system can be represented as a state-space model normalized by the input and frequency and composed by unit-less parameters in the format:

$$\frac{d\mathbf{e}(\omega t)}{d\omega t} = \overline{\mathbf{A}}_N \mathbf{e}(\omega t) + \overline{\mathbf{B}}_N \frac{F_0}{F_0} u(\omega t) \quad (25)$$

and

$$\mathbf{y}(\omega t) = \overline{\mathbf{C}}_N \mathbf{e}(\omega t) + \overline{\mathbf{D}}_N \frac{F_0}{F_0} u(\omega t) \quad (26)$$

Being $\overline{\mathbf{A}}_N$, $\overline{\mathbf{B}}_N$, $\overline{\mathbf{C}}_N$ and $\overline{\mathbf{D}}_N$ the state, input, output and transmission unit-less matrices. Also, $F_0 u(\omega t)$ and $\mathbf{e}(\omega t)$ represent input source and the new vector space related to ωt , respectively. The unit-less matrices are represented by:

$$\overline{\mathbf{A}}_N = \begin{pmatrix} 0 & \Omega & 0 \\ \Omega & -2\zeta\Omega & -\Phi\Omega \\ 0 & \Phi\Omega & -\frac{\Omega}{Q_m} \end{pmatrix}, \quad (27)$$

$$\overline{\mathbf{B}}_N = \begin{pmatrix} 0 \\ -1 \\ 0 \end{pmatrix} \quad (28)$$

and

$$\overline{\mathbf{C}}_N = \begin{pmatrix} \frac{Q_m a \Omega^2}{\Lambda^2} & 0 & 0 \\ 0 & 0 & \Lambda \end{pmatrix}. \quad (29)$$

The input is $\frac{F_0}{F_0} u(\omega t)$, in which the signal amplitude is normalized and $u(\omega t)$ is the input function. In addition, $\overline{\mathbf{D}}_N = 0$.

III. EVALUATION OF THE PIEZOELECTRIC NORMALIZED SYSTEM

The system described by (25) and (26) is suitable for parameter sweeping due to well-defined limit values for the unit-less parameters. Also, it can be analyzed by mathematical softwares. The normalized mechanical resonant frequency Ω can be swept between 0.1 and 2.0; in this case, 1.0 means the operation in resonance frequency. There are several possibilities to evaluate the normalized piezoelectric model. For example, considering a set of Q_m and fixed values for ζ and Φ , a parameter sweep can be performed in Ω and Λ . Another possibility is evaluating different values of Φ for fixed normalized resonance frequencies.

The inverse system's transfer power ratio a needs a numerical value, which can be calculated by [29]:

$$T_{POT} = \frac{1}{a} = \frac{1}{2\pi} \int_0^{2\pi} \left[\frac{v_{R_L}(\omega t)}{F_0} \right]^2 d\omega t. \quad (30)$$

Being T_{POT} the transfer power ratio. In this section, some theoretical results are shown in Fig. 4 regarding to the aforementioned features of the normalized piezoelectric system. The input function is considered $u(\omega t) = \sin(\omega t)$. For fixed values: $\Phi = 0.1$, $\zeta = 0.05$, $Q_m = 10$, a parameter sweep was performed in Ω from 0.1 to 2.0 with steps of 0.01; the transfer power ratio was calculated for each step and the result is shown in Fig. 4(a). The same procedure was performed considering $\Phi = 0.5$, which is depicted in Fig. 4(b). The transfer power ratio T_{POT} as function of Ω is depicted in Fig. 4(c) for different values of ζ considering $\Lambda = 1.0$ and $Q_m = 10$ and in Fig. 4(d) for $\Lambda = 0.8$ and $Q_m = 200$. The transfer power ratio T_{POT} as function of Ω and Φ for $Q_m = 10$, $\Lambda = 1.0$ and $\zeta = 0.05$ is depicted in a 3D chart in Fig. 4(e). Also, the output rms voltage $V_{R_L(rms)}$ as function of Φ and Ω for $Q_m = 10$, $\Lambda = 1.0$ and $\zeta = 0.05$, the transfer power ratio T_{POT} as function of Λ and Ω for $Q_m = 10$ and $\Phi = 0.5$, the output rms voltage $V_{R_L(rms)}$ as function of Λ and Ω for $Q_m = 10$ and $\Phi = 0.5$ are shown in Fig. 4(f), 4(g) and 4(h), respectively. It can be seen that the transfer power ratio is higher when Λ and/or Ω is closer to 1.0. Also the $V_{R_L(rms)}$ linear increases when Φ increases. For lower values of ζ , the transfer power ratio is higher. The maximum transfer power ratio is dependent of the coupling factor as depicted in Fig. 4(i) and Fig. 4(j). The influence of Λ is shown in the phase diagrams in Fig. 4(k) and Fig. 4(l). These diagrams are called work-cycles and relate the output variables. The larger the enclosed area, more energy are transferred. As an aside note, there several possibilities to analyze the behavior of the system by using the unit-less

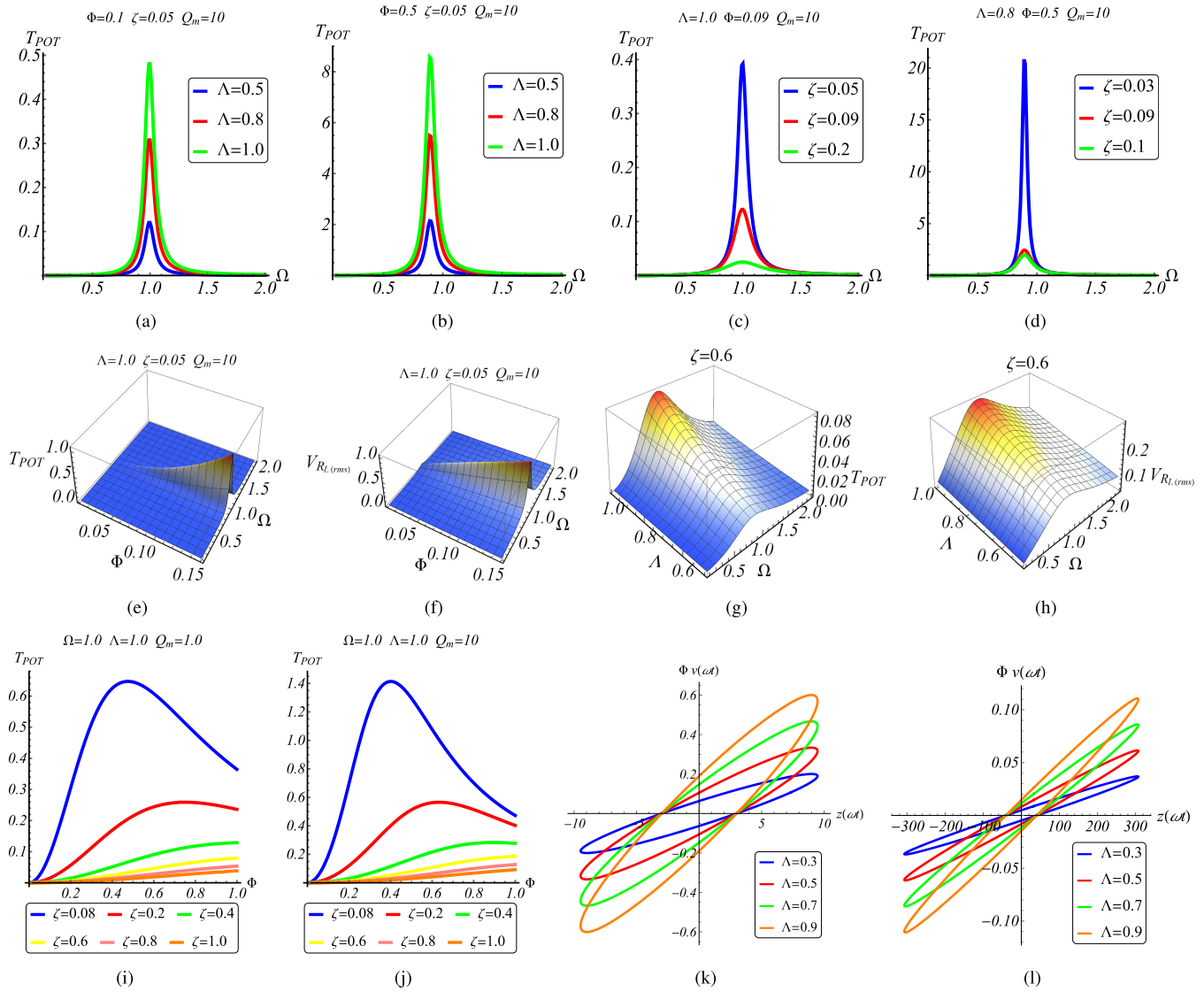


Fig. 4. Normalized theoretical results. (a) Transfer power ratio T_{POT} as function of the normalized mechanical resonance frequency Ω for $Q_m = 10$, $\zeta = 0.05$ and $\Phi = 0.1$. (b) Transfer power ratio T_{POT} as function of the normalized mechanical resonance frequency Ω for $Q_m = 10$, $\zeta = 0.05$ and $\Phi = 0.5$. (c) Transfer power ratio T_{POT} as function of the normalized mechanical resonance frequency Ω for $Q_m = 10$, $\Phi = 0.09$ and $\Lambda = 1.0$. (d) Transfer power ratio T_{POT} as function of the normalized mechanical resonance frequency Ω for $Q_m = 200$, $\Phi = 0.5$ and $\Lambda = 0.8$. (e) Transfer power ratio T_{POT} as function of coupling factor Φ and normalized mechanical resonance frequency Ω for $Q_m = 10$, $\Lambda = 1.0$ and $\zeta = 0.05$. (f) Output rms voltage $V_{R_L(rms)}$ as function of coupling factor Φ and normalized mechanical resonance frequency Ω for $Q_m = 10$, $\Lambda = 1.0$ and $\zeta = 0.05$. (g) Transfer power ratio T_{POT} as function of normalized electromechanical resonance frequency Λ and normalized mechanical resonance frequency Ω for $Q_m = 10$ and $\Phi = 0.5$. (h) Output rms voltage $V_{R_L(rms)}$ as function of normalized electromechanical resonance frequency Λ and normalized mechanical resonance frequency Ω for $Q_m = 10$ and $\Phi = 0.5$. (i) Transfer power ratio T_{POT} as function of coupling factor Φ for $Q_m = 1$. (j) Transfer power ratio T_{POT} as function of coupling factor Φ for $Q_m = 10$. (k) Work-cycle for $\Omega = 1.0$, $\zeta = 0.1$, $Q_m = 3$ and $\Phi = 0.5$. (l) Work-cycle for $\Omega = 0.4$, $\zeta = 0.1$, $Q_m = 3$ and $\Phi = 0.5$.

parameters, in this section, some of the possibilities were presented.

IV. REAL SYSTEM PARAMETERS AND RELATIONSHIPS AMONG PIEZO-HARVESTER DOMAINS

The theoretical results achieved in previous sections are interesting because they show the possibility of several parameter sweeping using unit-less parameters to evaluate the general behavior of the system. However, it does not make sense if the unit-less parameters are not associated with real system parameters. In this section, four domains for the piezo-harvester representation are described by means of

relationships among them. First, the relations among electro-mechanical, unit-less and piezoelectric parameters are shown in Table I. The piezoelectric parameters are described based on the constitutive equations of piezoelectricity [30]. The piezoelectric parameters are: stiffness of the piezoelectric material c_{33}^E , piezoelectric material coupling constant e_{33} , permittivity of the piezoelectric layer ϵ_{33}^S , area A and piezoelectric layer thickness T_p . The unit-less-based equations are derived based on (20), (21), (22), (23), (24) and the piezoelectric equations from Table I. Furthermore, it can be interesting to represent the system by means of electrical circuit parameters in order to use circuit simulation tools to evaluate the system.

TABLE I
RELATIONSHIPS AMONG PIEZO-HARVESTER DOMAINS I

Electromechanical	Unit-less	Piezoelectric
M	$M = \frac{R_L \Omega}{\omega Q_m \Lambda^2}$	M
K	$K = \frac{\omega R_L \Omega^3}{Q_m \Lambda}$	$K = \frac{c_{33}^E A}{T_p}$
C_o	$C_o = \frac{Q_m}{\omega R_L \Omega}$	$C_o = \frac{\epsilon_{33}^S A}{T_p}$
α	$\alpha = \frac{\Omega \Phi}{\Lambda}$	$\alpha = \frac{\epsilon_{33}^A}{T_p}$
D	$D = \frac{2\zeta \Omega^2 R_L}{Q_m \Lambda^2}$	D

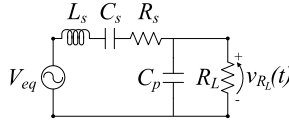


Fig. 5. Equivalent electrical circuit.

TABLE II
RELATIONSHIPS AMONG PIEZO-HARVESTER DOMAINS II

Electrical circuit	Electromechanical	Unit-less	Piezoelectric
L_s	$L_s = \frac{M}{\alpha^2}$	$L_s = \frac{R_L}{\omega Q_m \Omega \Phi}$	$L_s = \frac{M T_p^2}{\epsilon_{33}^2 A^2}$
C_s	$C_s = \frac{\alpha^2}{K}$	$C_s = \frac{Q_m \Phi^2}{\omega R_L \Omega \Lambda}$	$C_s = \frac{\epsilon_{33}^2 A}{c_{33}^2 T_p}$
C_p	$C_p = C_o$	$C_p = \frac{Q_m}{\omega R_L \Omega}$	$C_p = \frac{\epsilon_{33}^S A}{T_p}$
R_s	$R_s = \frac{D}{\alpha^2}$	$R_s = \frac{2\zeta R_L}{Q_m \Phi^2}$	$R_s = \frac{c_{33}^T T_p^2}{\epsilon_{33}^2 A^2}$
V_{eq}	$V_{eq} = \frac{F_0}{\alpha}$	$V_{eq} = \frac{F_0 \Lambda}{\Omega \Phi}$	$V_{eq} = \frac{F_0 T_p}{\epsilon_{33} A}$

The piezo-harvester can be represented as a electrical circuit as depicted in Fig. 5, being L_s the equivalent series inductor, C_s the equivalent series capacitance, C_p the equivalent parallel capacitor, R_s the equivalent series capacitor and V_{eq} the equivalent input source. Relationships among electrical circuit, electromechanical, unit-less and piezoelectric parameters are shown in Table II.

Equations in Tables I and II are used as interface between real system parameters and unit-less parameters. They can be used to extract the piezoelectric parameters based on the normalized theoretical results. Also, assuming a piezoelectric material the relationships among piezo-harvester domains can be used to find the unit-less parameters and evaluate the behavior of the system by means of parameter sweeping. The aforementioned relationships lead to a two-way design tool in piezo-harvester systems.

V. PIEZO-HARVESTER BASED ON CLASS-E RESONANT RECTIFIER

The piezoelectric harvester provides an AC signal as output voltage, which must be rectified in order to obtain a DC signal

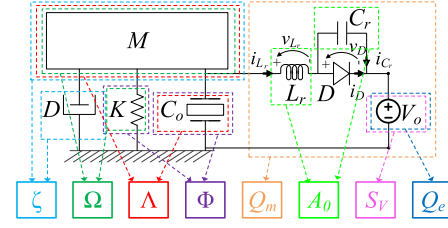


Fig. 6. Decomposition in unit-less parameters scheme for the piezo-harvester based on Class-E resonant rectifier.

to supply a load. Several works deal with many types of AC-DC converters [16], [17], [20], [33]. In this work, a piezo-harvester based on Class-E resonant rectifier is presented, which is a novelty in the literature. The Class-E resonant rectifier is a circuit that converts an AC signal to a DC signal by means of soft-switching of the rectifying diode, which reduces losses [34]. The analysis methodology is the same shown in Section II. The piezo-harvester based on Class-E resonant rectifier and the decomposition in unit-less parameters scheme are depicted in Fig. 6.

In Fig. 6, L_r and C_r are the reactive components, D is the diode, V_0 an equivalent voltage source and i_{L_r} , i_{C_r} , i_D , v_{L_r} , and v_D are the circuit variables. New unit-less parameters are described by: normalized resonant frequency A_0 , AC-to-DC transfer function S_V and electrical quality factor Q_e . These parameters are equated by:

$$A_0 = \frac{\omega_0}{\omega}; \quad \omega_0 = \frac{1}{\sqrt{L_r C_r}}, \quad (31)$$

$$S_V = \frac{V_0 \sqrt{2}}{V_{R_L}} \quad (32)$$

and

$$Q_e = \frac{R_0}{\omega_0 L_r} = \omega_0 C_r R_0. \quad (33)$$

In (32), V_{R_L} is the peak value of the output voltage provided by the piezoelectric element. Also, in (33), R_0 represents the AC-DC rectifier load that was replaced by V_0 . The main goal here is to obtain the transfer power ratio from the input force F_0 to the rectifier output voltage V_0 by using the methodology proposed in this work.

The Class-E resonant rectifier can be represented by a separated normalized state-space model on the form of (25) and (26). The interface between the piezoelectric component and the rectifier model is performed by setting the input of the rectifier as the output of the piezoelectric model. In this case, V_{R_L} and V_0 can be related by the inverse system's transfer power ratio b by $V_{R_L}/V_0 = bR_0$. In addition, V_0 is also an input, which characterizes a MIMO system.

By including the switched rectifier, the system becomes non-linear. In this case, state-space matrices are developed for each operating mode of the rectifier based on the diode duty cycle D_c : Mode 1 ($0 < t \leq D_c 2\pi$), D is off; Mode 2 ($D_c 2\pi < t \leq 2\pi$), D is on. The vector space is written as:

$$\mathbf{e}(t) = \left[\mathbf{i}_{L_r} \frac{\sqrt{L_r}}{\sqrt{2}}, \mathbf{v}_{C_r} \frac{\sqrt{C_r}}{\sqrt{2}} \right]^T. \quad (34)$$

The output vector and the input vector are described by:

$$\mathbf{y}(\omega t) = \left[\frac{\mathbf{i}_{L_r}(\omega t)}{\mathbf{I}_{R_L}}, \frac{\mathbf{v}_{in}(\omega t)}{\mathbf{V}_{R_L}}, \frac{\mathbf{v}_{C_r}(\omega t)}{\mathbf{V}_{R_L}}, \frac{\mathbf{V}_o}{\mathbf{V}_{R_L}} \right]^T \quad (35)$$

and

$$\mathbf{u}(\omega t) = [\mathbf{V}_{R_L} \mathbf{v}_{R_L}(\omega t), \mathbf{V}_o]^T. \quad (36)$$

The normalized state-space model for the Class-E resonant rectifier is given by: $\overline{\mathbf{A}}_{N1} = \begin{pmatrix} 0 & -A_0 \\ A_0 & 0 \end{pmatrix}$, $\overline{\mathbf{B}}_{N1} = \begin{pmatrix} 1 & -1 \\ 0 & 0 \end{pmatrix}$, $\overline{\mathbf{A}}_{N2} = \begin{pmatrix} 0 & 0 \\ 0 & 0 \end{pmatrix}$, $\overline{\mathbf{B}}_{N2} = \begin{pmatrix} 1 & -1 \\ 0 & 0 \end{pmatrix}$, $\overline{\mathbf{C}}_{N1} = \overline{\mathbf{C}}_{N2} = \begin{pmatrix} A_0 Q_e b & 0 & 0 & 0 \\ 0 & 0 & A_0 & 0 \end{pmatrix}^T$ and $\overline{\mathbf{D}}_{N1} = \overline{\mathbf{D}}_{N2} = \begin{pmatrix} 0 & 1 & 0 & 0 \\ 0 & 0 & 0 & 1 \end{pmatrix}^T$.

In (36), $v_{R_L}(\omega t)$ is the output response from the piezoelectric element system. This is used as one of the inputs for the rectifier state-space model. As long as the system has two state-space representations (one for each operating mode), the mode 1 should be solved analytically by considering initial conditions $i_{L_r}(0)$ and $v_{C_r}(0)$ symbolically. Subsequently, the results for mode 1 should be used as initial conditions to solve the mode 2. Finally, the solution of mode 2 is equated to the initial conditions, which allows solving a linear system in order to find the unit-less parameters in the same way of Section III. In order to evaluate the system when considering the Class-E rectifier, the following parameters should be mentioned:

- Piezoelectric element transfer power ratio: $T_{POT} = (V_{R_L}/F_0)^2$;
- Class-E resonant rectifier transfer power ratio: $T_{(V_{R_L}-V_0)} = (V_0/V_{R_L})^2$;
- Overall transfer power ratio $T_{(V_0-F_0)} = (V_0/F_0)^2$.

A parameter sweep on duty cycle D_c from 0.1 to 0.85 was performed to evaluate the piezo-harvester based on Class-E resonant rectifier for $\Omega = 0.8$, $\Omega = 1.0$ and $\Omega = 1.2$. The transfer power ratio was evaluated for each point based on the following unit-less parameters: $\Lambda = 0.33$, $\Phi = 0.4$, $\zeta = 0.2$ and $Q_m = 10$. The Class-E rectifier transfer power ratio $T_{(V_{R_L}-V_0)}$ as function of the diode duty cycle D_c and as function of the normalized resonant frequency A_0 are shown in Fig. 7(a)-(b). The overall transfer power ratio $T_{(V_0-F_0)}$ as function of D_c and as function of A_0 are shown in Fig. 8(a)-(b). The rectifier was considered as the load R_L of the piezoelectric element. In this case, the analysis is under the following assumption for impedance matching: $R_L = Z_{in} = R_0/S_V^2$, being Z_{in} the rectifier input impedance. This leads to the following:

$$S_V^2 = \frac{R_0}{R_L} \left\{ \frac{C_o C_r \omega \omega_0}{C_o C_r \omega \omega_0} \right\} S_V^2 = \frac{Q_e \omega_m C_o}{Q_m \omega_0 C_r} \quad (37)$$

$$\left\{ \frac{\omega}{\omega_0} \right\} S_V^2 = \frac{Q_e \Omega C_o}{Q_m A_0 C_r}. \quad (37)$$

Defining the capacitances ratio as $C_o/C_r = \gamma$, the unit-less relationship is achieved:

$$\gamma = S_V^2 \frac{Q_m A_0}{Q_e \Omega}. \quad (38)$$

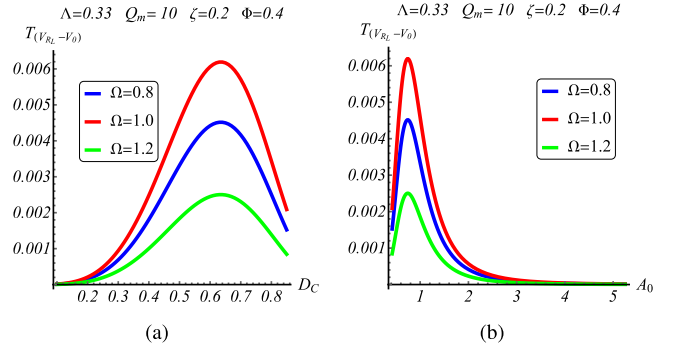


Fig. 7. Class-E resonant rectifier transfer power ratio. (a) Transfer power ratio $T_{(V_{R_L}-V_0)}$ as function of diode duty cycle D_c . (b) Transfer power ratio $T_{(V_{R_L}-V_0)}$ as function of normalized resonant frequency A_0 .

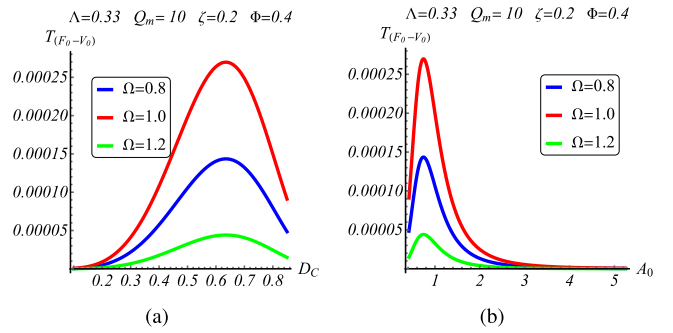


Fig. 8. Overall transfer power ratio. (a) Transfer power ratio $T_{(V_0-F_0)}$ as function of diode duty cycle D_c . (b) Transfer power ratio $T_{(V_0-F_0)}$ as function of normalized resonant frequency A_0 .

TABLE III
PIEZOELECTRIC PARAMETERS AND SPECIFICATIONS

Parameters / Specification	Value
Load, R_L	30 k Ω
Piezoelectric stiffness, c_{33}^E	8040 N \cdot m $^{-2}$
Piezoelectric coupling constant, e_{33}^E	0.0087 $\times 10^{-12}$ m \cdot V $^{-1}$
Permittivity of the layer, ϵ_{33}^E	2.8 $\times 10^{-6}$ F \cdot m $^{-1}$
Layer thickness, T_p	0.1 m
Area, A	78.5 mm 2
Mass, M	1 $\times 10^{-10}$ g
Input excitation amplitude, F_0	5 $\times 10^{-6}$ N
Input source frequency, f	40 kHz
Normalized mechanical frequency, Ω	1.0
Mechanical quality factor, Q_m	16

VI. RESULTS

An experimental validation were performed to verify the theoretical results. Considering a piezoelectric component with parameters and design specifications shown in Table III, the electromechanical, unit-less and circuit parameters were calculated by means of the relationships among piezo-harvester domains shown in Tables I and II and are described in Table IV. The normalized mechanical frequency $\Omega = 1.0$ is considered a specification because it is a desirable design

TABLE IV
ELECTROMECHANICAL, UNIT-LESS AND ELECTRICAL CIRCUIT PARAMETERS

Parameters	Value	Domain
Mechanical damping coefficient, D	$8.64 \times 10^{-7} N \cdot s \cdot m^{-1}$	Electromechanical
Mechanical stiffness, K	$6.31 N \cdot m^{-1}$	Electromechanical
Piezoelectric capacitance, C_o	$2.2 nF$	Electromechanical
Force factor, α	$6.89 \times 10^{-6} N \cdot V^{-1}$	Electromechanical
Coupling factor, Φ	0.05	Unit-less
Damping factor, ζ	0.017	Unit-less
Series inductor, L_s	$58 mH$	Electrical circuit
Series capacitance, C_s	$300 pF$	Electrical circuit
Series resistance, R_s	$1.8 k\Omega$	Electrical circuit
Parallel capacitance, C_o	$2.2 nF$	Electrical circuit
Equivalent input source, V_{eq}	$0.725 V$	Electrical circuit

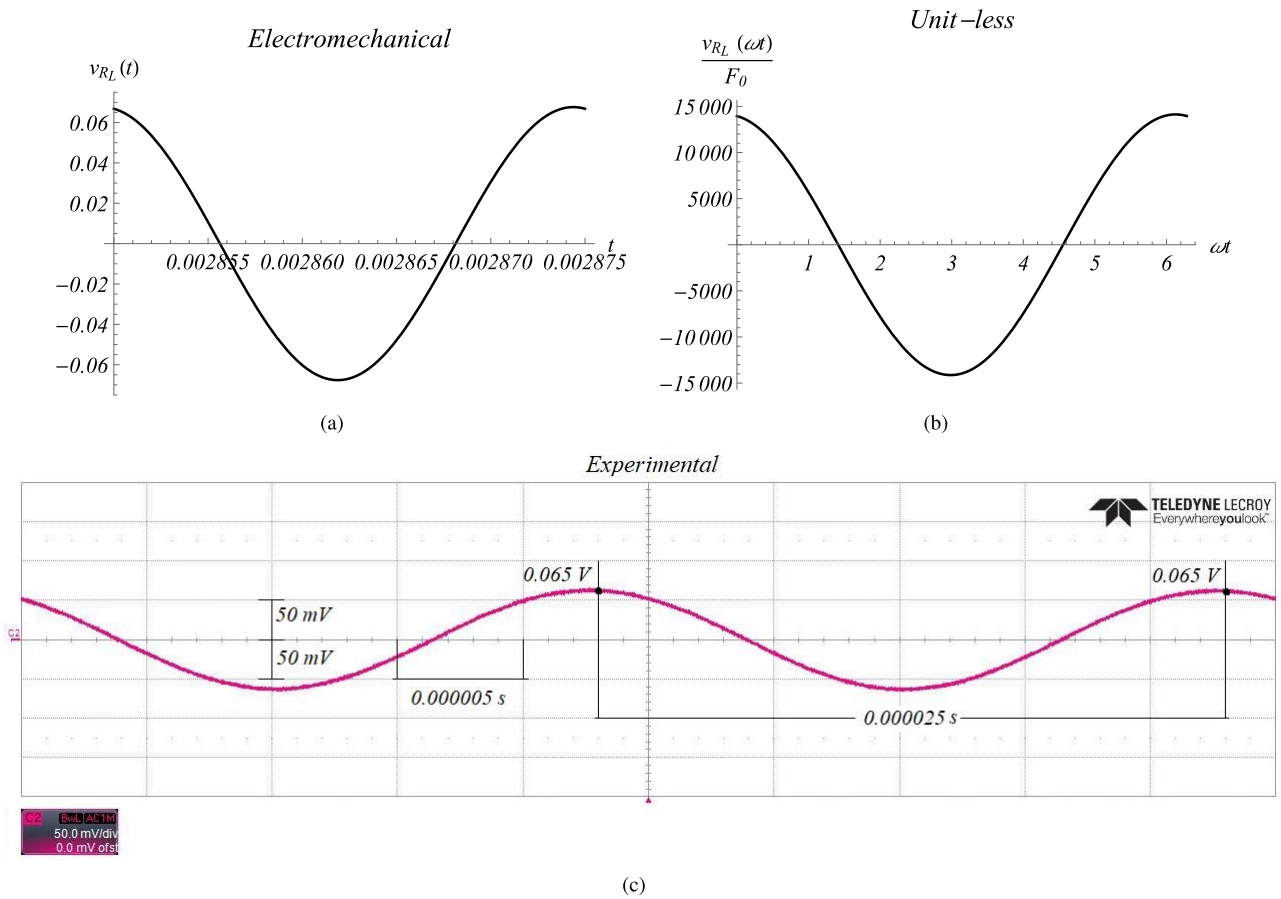


Fig. 9. Results for output voltage v_{RL} . (a) Electromechanical model. (b) Unit-less model. (c) Experimental validation (50 mV/div; 5 μ s/div).

point due to the maximum transfer power ratio as shown in the previous sections.

Considering the parameters and specifications shown in Tables III and IV, the electromechanical system described by equation (8) and the unit-less system in (25) and (26) were solved numerically by means of mathematical software. Also, the circuit in Fig. 5 was implemented in order to obtain experimental results. The results for the output voltage v_{RL} are

shown in Fig. 9. The theoretical results for the electromechanical and unit-less systems are depicted in Fig. 9(a) and Fig. 9(b) respectively. By multiplying unit-less waveform by F_0 it must be equal to the electromechanical result in relation to the y-axis, which is in agreement. Also, the experimental result in Fig. 9(c) is in accordance with the theoretical results. In order to verify the system response in a general way, the system transfer function that relates the output voltage

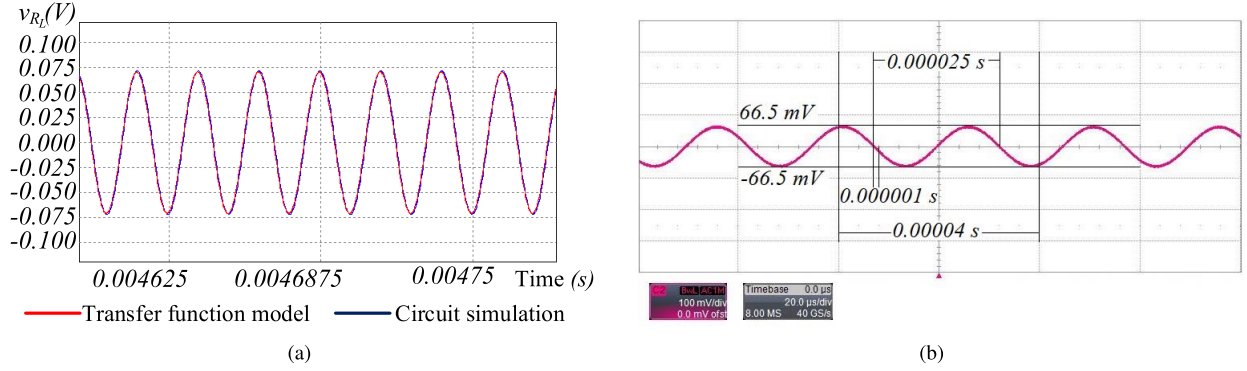


Fig. 10. Comparison among transfer function response, circuit simulation and experimental result. (a) Model validation. (b) Experimental output voltage (100 mV/div; 20 μs/div).

TABLE V
PIEZO-HARVESTER BASED ON CLASS-E RESONANT RECTIFIER - PARAMETERS AND SPECIFICATIONS

Parameters / Specification	Value
Input excitation amplitude, F_0	$89.5 \times 10^{-6} N$
Normalized resonant frequency, A_0	0.47
AC-to-DC transfer function, S_V	0.148
Electrical quality factor, Q_e	3
Resonant inductor, L_r	68 mH
Resonant capacitor, C_r	1 nF
Output filter capacitor, C_f	4.7 μF
Rectifier load, R_0	24 kΩ

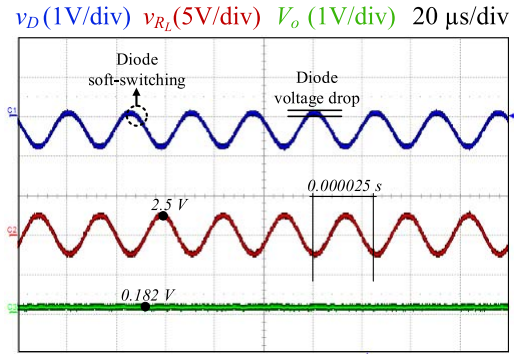


Fig. 11. Experimental results for the piezo-harvester based on Class-E resonant rectifier.

$V_{R_L}(s)$ and the input $F(s)$ is extracted from (8):

$$\frac{V_{R_L}(s)}{F(s)} = -\frac{3.107 \times 10^{13}s}{s^3 + 23802s^2 + 6.350 \times 10^{10}s + 9.574 \times 10^{14}}. \quad (39)$$

This transfer function is considered the model of the system and its response is compared with the electrical circuit response (simulation software) and with experimental results as shown in Fig. 10. A comparison of the transfer function model response and the output voltage from the circuit simulation is depicted in Fig. 10(a). Also, it can be seen that the experimental output voltage shown in detail in Fig. 10(b) is in agreement with the theoretical and simulation results. In order to experimentally verify the theoretical results in Fig. 7 and Fig. 8, the Class-E resonant rectifier was cascaded to the piezoelectric component. As long as diode voltage drop of the rectifier limits its input voltage operation, the input excitation amplitude was considered as 0.000089.5 N. The Class-E resonant rectifier parameters and specifications are presented in Table V and the experimental results in Fig. 11. The measurements for v_D , v_{R_L} and V_o are shown in Fig. 11, in which the diode soft-switching and the diode voltage drop are highlighted.

The quantitative results for the piezo-harvester based on Class-E resonant rectifier are shown in Table VI in order to compare the theoretical approach from Section V with the measurements in Fig. 11. Experimental value of $T_{(F_0-V_0)}$ becomes unit-less by multiplying α^2 .

TABLE VI
QUANTITATIVE RESULTS

Parameter	Theoretical	Experimental
Class-E transfer power ratio, $T_{(V_{R_L}-V_0)}$	0.00582	0.00535
Overall transfer power ratio, $T_{(F_0-V_0)}$	0.00023	0.00019

VII. COMPARISON WITH RELATED WORKS

In order to evaluate the developed methodology, this work is going to be compared with others by means of qualitative factors described by:

- 1) Type of representation: Defines the type of representation that is used as a starting point to analyze the system;
- 2) Methodology: Describes the method used to obtain and represent the model related to the system;
- 3) Evaluated parameters: Indicates if the parameters used to evaluate the response of the model are the real system components or unit-less and which parameters were evaluated;
- 4) Evaluated blocks: Indicates which blocks of the energy harvesting general representation are considered in the system modeling.

The qualitative comparison with related works are shown in Table VII. Regarding to the type of representation, an electrical equivalent circuit is used in [17]. It represents the piezoelectric component as a piezo-patch energy harvester in which a velocity proportional current in parallel to an

TABLE VII
QUALITATIVE COMPARISON

Work	Type of representation	Methodology	Evaluated parameters	Evaluated blocks
[16]	Electromechanical	Transfer function	Φ, Q_m, T_{POT}, η	Harvester AC-DC Converter
[17]	Electrical circuit	Circuit equations	Real system parameters	Harvester AC-DC Converter
[19]	Euler-Bernoulli beam	Governing equations of motion	Real system parameters	Input Harvester
[20]	Unimorph cantilevered	Governing equations of motion	Normalized displacement Normalized strain Real electrical power	Harvester AC-DC Converter
[24]	Real system properties	Finite element method	Real system parameters	Harvester
[26]	Electromechanical	Circuit equations	Real system parameters	Harvester Load
[27]	Unimorph cantilevered	Governing equations of motion	$\Omega, \Phi, \zeta, Q_m, \eta$	Harvester
[31]	Electromechanical	State-space modeling	Real system parameters	Harvester
[32]	Tapered cantilever	Governing equations of motion	Real system parameters	Harvester
[33]	Electrical circuit	Circuit equations	Real system parameters	Harvester AC-DC Converter
Present work	Electromechanical	State-space normalized modeling	$\Omega, \Lambda, \Phi, \zeta, Q_m, T_{POT}$	Harvester AC-DC Converter

equivalent piezoelectric capacitance is used. The present work and [16], [26], [31] use the electromechanical representation and [32] resorts to the cantilever characterization. Real system parameters are used in [17], [19], [24], [26], [31]–[33]. The methodology used in [16] is related to the obtainment of transfer functions based on unit-less parameters. The symbols used in [16] and [27] are not the same used in this work, however, they represent the same parameter. The symbols used in this paper are going to be used for the comparison. Therefore, it can be seen that unit-less parameters are used in [16], however, it does not consider the normalized electromechanical resonance frequency Λ and the damping factor ζ on the results. Also, the normalized mechanical resonance frequency is simplified as $\Omega = 1$. Within this scope, it has been shown in Fig. 4(d) that the maximum transfer power ratio is not achieved considering $\Omega = 1$ in certain cases. In addition, [16], [17], [20], [33] and the present work have the merit of analyzing the harvester and the AC-DC converter blocks. In [19], the input is analyzed in relation to the type of excitation. In addition, a normalized efficiency η is used in [16].

VIII. CONCLUSION

In this paper, a normalized analysis methodology for piezoelectric energy harvester systems was described. Considering several building blocks, such as input source, harvester, power

converters and load, which compose a harvesting system, it is necessary to evaluate them by taking into account a compromise between accuracy, complexity and effort. In this sense, this paper aimed to describe a methodology to represent the piezo-harvester system in four domains: electromechanical, normalized, real system parameters and electrical circuit. It was shown that the electromechanical model is used as a first approach to create an interface between the real system and a mathematical representation. The normalized model is suitable for parameter sweeping due to the general representation based on unit-less parameters. However, it is necessary to convert the unit-less terms into real system parameters. In this case, relationships among the piezo-harvester domains were derived. In order to provide a systematic methodology, an equivalence transformation technique and a decomposing in unit-less parameters scheme were used to easily make the conversion between models and to provide a model for a piezo-harvester based on Class-E resonant rectifier. The electromechanical, unit-less and electrical circuit models were compared considering piezoelectric parameters by means of theoretical, simulation and experimental results. Furthermore, the methodology described in this work was compared with related works in a qualitative way. Considering the research for new solutions in several applications, especially energy harvesting systems, the proposed work can be an useful

tool to analyze the system in a general way and to provide relationships among different types of system representation that can be used in different computational tools.

ACKNOWLEDGMENT

The authors would like to thank the national council for scientific and technological development (CNPq) and the Fraunhofer Institute for Integrated Circuits, Division Engineering of Adaptive Systems for technical and scientific support.

REFERENCES

- [1] W. Heywang, K. Lubitz, and W. Wersing, *Piezoelectricity* (Springer Series in Materials Science). Berlin, Germany: Springer, 2008.
- [2] S. Guerin, S. A. M. Tofail, and D. Thompson, "Longitudinal piezoelectricity in natural calcite materials: Preliminary studies," *IEEE Trans. Dielectr. Electr. Insul.*, vol. 25, no. 3, pp. 803–807, Jun. 2018.
- [3] M. Wahbah and B. Mohammad, "Piezo electric energy harvester and its interface circuit: Opportunities and challenges," in *Proc. IEEE 20th Int. Conf. Electron., Circuits, Syst.*, Dec. 2013, pp. 795–798.
- [4] K. V. Allamraju and K. Srikanth, "State of art: Piezoelectric vibration energy harvesters," in *Proc. 5th Int. Conf. Mater. Process. Characterization*, 2017, vol. 4, no. 2, pp. 1091–1098.
- [5] M. Krishnasamy and T. R. Lenka, "Analytical model with two degree of freedom of piezo-magneto-elastic energy harvester for low-frequency wide bandwidth applications," *IET Micro Nano Lett.*, vol. 13, pp. 857–861, Jun. 2018.
- [6] N. Wu, Q. Wang, and X. Xie, "Ocean wave energy harvesting with a piezoelectric coupled buoy structure," *Appl. Ocean Res.*, vol. 50, pp. 110–118, Mar. 2015.
- [7] A. Robichaud, P.-V. Cicek, D. Deslandes, and F. Nabki, "Frequency tuning technique of piezoelectric ultrasonic transducers for ranging applications," *J. Microelectromech. Syst.*, vol. 27, no. 3, pp. 570–579, Jun. 2018.
- [8] A. Robichaud, D. Deslandes, P.-V. Cicek and F. Nabki, "A novel topology for process variation-tolerant piezoelectric micromachined ultrasonic transducers," *J. Microelectromech. Syst.*, vol. 27, no. 6, pp. 1204–1212, Dec. 2018.
- [9] G. P. L. Thomas, J.-Y. Chapelon, J.-C. Béra, and C. Lafon, "Parametric shape optimization of lens-focused piezoelectric ultrasound transducers," *IEEE Trans. Ultrason., Ferroelectr., Freq. Control*, vol. 65, no. 5, pp. 844–850, May 2018.
- [10] F. Akasheh, J. D. Fraser, S. Bose, and A. Bandyopadhyay, "Piezoelectric micromachined ultrasonic transducers: Modeling the influence of structural parameters on device performance," *IEEE Trans. Ultrason., Ferroelectr., Freq. Control*, vol. 52, no. 3, pp. 455–468, Mar. 2005.
- [11] R. Sriramdas and R. Pratap, "An experimentally validated lumped circuit model for piezoelectric and electrodynamic hybrid harvesters," *IEEE Sensors J.*, vol. 18, no. 6, pp. 2377–2384, Mar. 2017.
- [12] T. A. Kosierkiewicz, "Piezoelectric shoe insert," U.S. Patent 8569935 B1, Oct. 29, 2013.
- [13] L. J. Radziemski, "Bio-implantable ultrasound energy capture and storage assembly including transmitter and receiver cooling," U.S. Patent 8082041 B1, Dec. 12, 2011.
- [14] W.-C. Lin, K.-Y. Lo, C.-L. Pan, and J.-W. Yang, "The performance comparison of greinacher rectifiers for wireless power transmission," *WIT Trans. Eng. Syst.*, vol. 88, pp. 237–244, Apr. 2014.
- [15] E. Belal, H. Mostafa, and M. S. Said, "Comparison between active AC-DC converters for low power energy harvesting systems," in *Proc. 27th Int. Conf. Microelectron.*, Dec. 2015, pp. 253–256.
- [16] X. Wang and L. Lin, "Dimensionless optimization of piezoelectric vibration energy harvesters with different interface circuits," *Smart Mater. Struct.*, vol. 22, no. 8, 2013, Art. no. 085011.
- [17] A. Aghakhani and I. Basdogan, "Equivalent impedance electroelastic modeling of multiple piezo-patch energy harvesters on a thin plate with AC-DC conversion," *IEEE/ASME Trans. Mechatronics*, vol. 22, no. 4, pp. 1575–1584, Aug. 2017.
- [18] H. Salmami, G. H. Rahimi, and S. A. H. Kordkheili, "An exact analytical solution to exponentially tapered piezoelectric energy harvester," *Shock Vib.*, vol. 2015, Apr. 2015, Art. no. 426876.
- [19] A. Erturk and D. J. Inman, "A distributed parameter electromechanical model for cantilevered piezoelectric energy harvesters," *J. Vib. Acoust.*, vol. 130, Jan. 2008, Art. no. 041002.
- [20] A. Erturk P. A. Tarazaga, J. R. Farmer, and D. J. Inman, "Effect of strain nodes and electrode configuration on piezoelectric energy harvesting from cantilevered beams," *J. Vib. Acoust.*, vol. 131, Jan. 2009, Art. no. 011010.
- [21] S. R. Anton, A. Erturk, and D. J. Inman, "Bending strength of piezoelectric ceramics and single crystals for multifunctional load-bearing applications," *IEEE Trans. Ultrason., Ferroelectr., Freq. Control*, vol. 59, no. 6, pp. 1085–1092, Jun. 2012.
- [22] A. D. T. Elliott and P. D. Mitcheson, "Power density improvement of a piezoelectric energy harvester through use of a micropower switch-mode interface," in *Proc. IEEE Sensors*, Oct. 2012, pp. 1–4.
- [23] T. Kasuga, "Design of a lane marker lighting system using piezoelectric bimorph modules," in *Proc. 8th EUROSIM Congr. Modelling Simulation*, 2013, pp. 633–636.
- [24] H.-C. Song *et al.*, "Ultra-low resonant piezoelectric MEMS energy harvester with high power density," *J. Microelectromech. Syst.*, vol. 26, no. 6, pp. 1226–1234, Dec. 2017.
- [25] C. Sugino, M. Ruzzene, and A. Erturk, "Design and analysis of piezoelectric metamaterial beams with synthetic impedance shunt circuits," *IEEE/ASME Trans. Mechatronics*, vol. 23, no. 5, pp. 2144–2155, Oct. 2018.
- [26] S.-J. Huang, T.-S. Lee, and P.-L. Lin, "Application of piezoelectric-transformer-based resonant circuits for AC LED lighting-driven systems with frequency-tracking techniques," *IEEE Trans. Ind. Electron.*, vol. 61, no. 12, pp. 6700–6709, Dec. 2014.
- [27] R. Sriramdas and R. Pratap, "Scaling and performance analysis of MEMS piezoelectric energy harvesters," *J. Microelectromech. Syst.*, vol. 26, no. 3, pp. 679–690, Jun. 2017.
- [28] Y. C. Shu and I. C. Lien, "Analysis of power output for piezoelectric energy harvesting systems," *Smart. Mater. Struct.*, vol. 15, no. 6, pp. 1499–1512, Sep. 2006.
- [29] F. E. Bisogno, "Fakultät für elektrotechnik und informationstechnik der Technischen Universität Chemnitz-Zwickau," Ph.D. dissertation, Chemnitz, Germany, 2007. [Online]. Available: <https://books.google.com.br/books?id=hNdaMgAACAAJ>
- [30] N. E. Dutoit, B. L. Wardle, and S. Kim, "Design considerations for MEMS-scale piezoelectric mechanical vibration energy harvesters," *Integr. Ferroelectr.*, vol. 714, pp. 121–158, Aug. 2006.
- [31] A. Erturk and D. J. Inman, *Piezoelectric Energy Harvesting*. Hoboken, NJ, USA: Wiley, 2011.
- [32] W. U. Syed, A. Bojesomo, and I. M. Elfadel, "Electromechanical model of a tapered piezoelectric energy harvester," *IEEE Sensors J.*, vol. 18, no. 14, pp. 5853–5862, Jul. 2018.
- [33] S. Du, Y. Jia, C. Zhao, G. A. J. Amaratunga, and A. A. Seshia, "A passive design scheme to increase the rectified power of piezoelectric energy harvesters," *IEEE Trans. Ind. Electron.*, vol. 65, no. 9, pp. 7095–7105, Sep. 2018.
- [34] A. Ivascu, M. K. Kazimierczuk, and S. Birca-Galateanu, "Class E resonant low dv/dt rectifier," *IEEE Trans. Circuits Syst. I, Fundam. Theory Appl.*, vol. 39, no. 8, pp. 604–613, Aug. 1992.



Lucas S. Mendonça was born in Santa Maria, Brazil, in 1993. He received the B.Sc. degree in control and automation engineering and the M.Sc. degree in electrical engineering from the Universidade Federal de Santa Maria, Brazil, in 2015 and 2017, respectively. He has been a Researcher with Fraunhofer IIS/EAS, Germany. He is also a member of the Doctorate Programs at the Universidade Federal de Santa Maria, and Brandenburgische Technische Universität Cottbus, Germany. He has experience in resonant power converters, resonant and PWM dc/dc power converters, dc/ac inverters, system modeling, low-power energy-harvesting systems, and contactless energy transfer systems.



Leandro T. Martins was born in Caxias do Sul, Brazil, in 1992. He received the B.Sc. degree in control and automation engineering and the M.Sc. degree in electrical engineering from the Federal University of Santa Maria (UFSM), Santa Maria, Brazil, in 2015 and 2018, respectively. He is currently pursuing the Cooperative Doctorate degree with UFSM, Brazil, and BTU Cottbus, Germany. He is also a Researcher with Fraunhofer IIS/EAS. His research interests include modeling and design

of dc-dc converters, control of static power converters, digital control techniques for power electronics, and control of grid-connected converters for distributed generation and renewable energy systems.



Matthias Radecker received the Dipl.Ing. degree in electrical engineering and the Dr.Ing. degree from the University of Chemnitz, Germany, in 1978 and 2000, respectively. He was responsible for power electronics and analog-mixed-signal circuit design at Fraunhofer IZM, Berlin. Since 2016, he has been with Fraunhofer EAS-IIS, Dresden. He holds patents in the area of resonant and capacitorless power conversion and has published related papers. His research interests include PSOC, lighting, digital power control, and piezoelectric applications.



Fábio E. Bisogno was born in Santa Maria, Brazil, in 1973. He received the B.S. and M.S. degrees in electrical engineering from the Federal University of Santa Maria (UFSM), Santa Maria, in 1999 and 2001, respectively, and the Dr.Ing. degree in electrical engineering from Technische Universität Chemnitz, Chemnitz, Germany, in 2006. From 2003 to 2009, he was a Research Engineer with the Institute for Autonomous Intelligent Systems and the Institute for Reliability and Microintegration, Fraunhofer. Since 2009, he has been a Professor with the Department of Electrical Energy Processing, UFSM. His research interests include resonant converters, electronic ballasts, self-oscillating systems, power supply miniaturization, piezoelectric transformers, sensitivity analysis, lighting systems, fluorescent lamp models, and power generation systems using internal combustion engines.



Dirk Killat (M'96) was born in Hanau, Germany, in 1966. He received the Diploma degree in electronic engineering and the Ph.D. degree from Technische Universität Darmstadt, Germany, in 1992 and 1997, respectively. Since 2008, he has been a Professor and the Chair for microelectronics with the Brandenburg University of Technology Cottbus-Senftenberg, Germany. He has been a member of the URSI Committee D, since 2013. He is a co-editor of *Advances in Radio Science*.